東北大学機関リポジトリ
TOUR
Tohoku University Repository

Linewidth of the Raman features of individual single-wall carbon nanotubes

Linewidth of the Raman features of individual single-wall carbon nanotubes

A. Jorio,[1,2] C. Fantini,[1] M. S. S. Dantas,[1] M. A. Pimenta,[1] A. G. Souza Filho,[3,6] Ge. G. Samsonidze,[4] V. W. Brar,[3]
G. Dresselhaus,[5] M. S. Dresselhaus,[3,4] A. K. Swan,[7] M. S. Ünlü,[7] B. B. Goldberg,[7,8] and R. Saito[9]

[1]*Departamento de Física, Universidade Federal de Minas Gerais, Belo Horizonte, MG, 30123-970 Brazil*
[2]*Department of Physics, Massachusetts Institute of Technology, Cambridge, Massachusetts 02139-4307*
[3]*Department of Physics, Massachusetts Institute of Technology, Cambridge, Massachusetts 02139-4307*
[4]*Department of Electrical Engineering and Computer Science, Massachusetts Institute of Technology,
Cambridge, Massachusetts 02139-4307*
[5]*Francis Bitter Magnet Laboratory, Massachusetts Institute of Technology, Cambridge, Massachusetts 02139-4307*
[6]*Departamento de Física, Universidade Federal do Ceará, Fortaleza–CE, 60455-760 Brazil*
[7]*Electrical and Computer Engineering Department, Boston University, Boston, Massachusetts 02215*
[8]*Department of Physics, Boston University, Boston, Massachusetts 02215*
[9]*Department of Electronic-Engineering, University of Electro-Communications, Tokyo, 182-8585 Japan*

In this work we analyze the room-temperature linewidth for several Raman features (i.e., the radial breathing mode, the G band, the D band, and the G' band) observed for individual isolated single-wall carbon nanotubes (SWNTs). Temperature-dependent measurements on SWNT bundles and isolated SWNTs show that anharmonic effects are not important for linewidth broadening at room temperature. Measurements on a large number of samples (170 isolated SWNTs) allow us to filter out the effect from extrinsic SWNT properties (e.g., defects, tube deformations, substrate roughness) and to obtain information about intrinsic properties related to phonon and electron dispersion relations, curvature and Breit-Wigner-Fano effects, single- vs double-resonance Raman scattering processes, and the resonance condition itself through a linewidth analysis. We also use observations at the single-nanotube level to understand linewidth effects in SWNT bundles.

I. INTRODUCTION

Single-wall carbon nanotubes (SWNTs) have been intensively studied because of the interesting physics arising from their one-dimensional (1D) behavior and because of their high potential for technological applications.[1,2] Resonance Raman spectroscopy is one of the main experimental techniques that have been used both to study the 1D physics of SWNTs and to characterize SWNT samples structurally.[3] The strong coupling between electrons and phonons in this 1D system gives rise to highly unusual resonance Raman spectra, allowing the observation of the Raman signal from one isolated SWNT, which makes it possible to gain new physical insights into 1D systems.[4]

Although many papers have been published discussing the resonance Raman spectroscopy of SWNTs,[3,4] there is to our knowledge only one systematic study until now (by Iliev *et al.*[5]) of the linewidth of the radial breathing mode (RBM) feature occurring in the SWNT Raman spectra, even though linewidth studies provide important insights into the physical mechanisms involved in each feature of the resonance Raman spectra. Iliev *et al.* performed a linewidth study of the RBM feature between 5 and 500 K, using a sample composed of SWNT bundles. They showed that a very small temperature dependence of the Raman linewidth is observed and that each of the low-frequency RBM Raman bands is a superposition of several narrower Raman lines corresponding to different (n,m) SWNTs with similar diameter (d_t). They found the value 3 cm^{-1} for the natural temperature-independent linewidth for the radial breathing mode.[6]

Several mechanisms (in addition to instrumental broaden-

ing) can be responsible for the observed linewidth broadening of the resonance Raman features in SWNTs: (i) temperature-dependent effects (anharmonic processes, phonon-phonon and electron-phonon scattering, and other effects); (ii) temperature-independent effects, which can be divided into (a) extrinsic SWNT properties, such as tube-tube–tube-substrate interactions, nanotube deformations, nanotube defects (vacancies, substitutional and interstitial impurities, 7-5 structural defects, etc.), and finite-size effects; (b) intrinsic SWNT properties connected with the SWNT diameter, phonon and electron dispersion relations, trigonal warping effects, whether the SWNT is metallic or semiconducting, and curvature effects; (c) the resonance condition of the Raman scattering for the specific SWNT, related to the energy separations between the incident or scattered photon and the pertinent electronic van Hove singularity, or the single- vs double-resonance nature of the Raman scattering process. In this paper we use the above notation to refer to specific linewidth broadening processes.

In this work we first discuss the temperature-dependent behavior of the Raman spectra in SWNT bundles and isolated SWNTs, showing that temperature-dependent effects [processes (i)] are not very important for the linewidth analysis at room temperature. Next, we discuss the insights given by the linewidth study of the temperature-independent line broadening in SWNTs at room temperature [processes (ii)]. We focus on the diameter (d_t) dependence of the linewidth for different resonant Raman features, including the RBM, the graphite-like G-band modes, and the disorder-induced D band and its second-order feature, the G' band [see Fig. 1 for
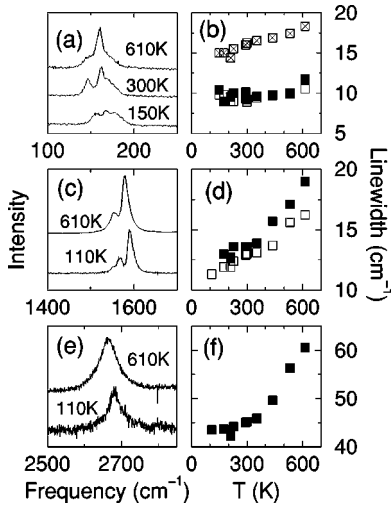
FIG. 1. (a) and (b) show, respectively, the RBM Raman spectra for SWNT bundles at different temperatures T and the RBM linewidth Γ_{RBM} dependence on temperature. Γ_{RBM} for the RBM features at about 150, 165, and 175 cm^{-1} is shown by solid squares, open squares, and crossed squares, respectively. (c) and (d) give corresponding Raman spectra and linewidths vs T for the G band. Solid squares give Γ_{G^+} for the peak at ~ 1590 cm^{-1} and open squares give Γ_{G^-} for the peak at ~ 1570 cm^{-1}. (e) and (f) describe the corresponding T-dependent data for the G' band at ~ 2670 cm^{-1}. Raman spectra are obtained with $E_{laser} = 2.41$ eV.

FIG. 2. (a) Raman spectra of one metallic (top) and of one semiconducting (bottom) isolated SWNT obtained with $E_{laser} = 1.58$ eV. The RBM, D,G, and G' bands are indicated, as well as features coming from the Si substrate. (b) FWHM linewidth Γ_{RBM} vs d_t for 81 metallic (solid symbols) and 89 semiconducting (open symbols) SWNTs at 290 K. Circles indicate data obtained with the 2.41 or 2.54 eV excitation laser lines and diamonds when obtained with a 1.58 eV laser. (c) Γ_{RBM} vs $E_{laser} - E_{ii}$ for metallic (solid symbols) and semiconducting (open symbols) in the range $1.4 < d_t < 1.8$ nm. Data are for $E_{laser} = 1.58$ eV and 2.41 eV.

SWNT bundles and Fig. 2(a) for isolated SWNTs on a Si/SiO$_2$ substrate].

The study presented here is based on measurements of the Raman spectra for 170 isolated SWNTs. Linewidth studies are best carried out at the single-nanotube level where the tube-tube interaction and superposition of different SWNT spectra do not occur. Then the broadening effects are minimized, and linewidths approaching the natural linewidths γ for the various Raman features should be achievable under appropriate conditions. However, we still must consider that linewidth measurements at the single-nanotube level are delicate, and here the use of a large number of tubes (170 different SWNTs) allows us to filter out the linewidth broadening due to extrinsic SWNT properties [processes (iia) in the previous paragraph], thereby providing information about intrinsic SWNT properties [processes (iib)] and about the resonance condition itself [process (iic)], as discussed above. We also use observations at the single-nanotube level to gain insights into linewidth effects in SWNT bundles.

The presentation of this paper is organized as follows: Section II discusses the experimental details, while Sec. III discusses temperature-dependent measurements on SWNT bundles and isolated SWNTs. Section IV discusses temperature-independent measurements carried out at room temperature on isolated SWNTs, and it is divided into subsections that discuss, separately, the RBM (Sec. IV A), the G band (Sec. IV B), and the D and G' bands (Sec. IV C). A summary is given in Sec. V.

II. EXPERIMENT

Isolated SWNTs were grown on a Si/SiO$_2$ substrate by the chemical vapor deposition (CVD) method.[7] Two samples
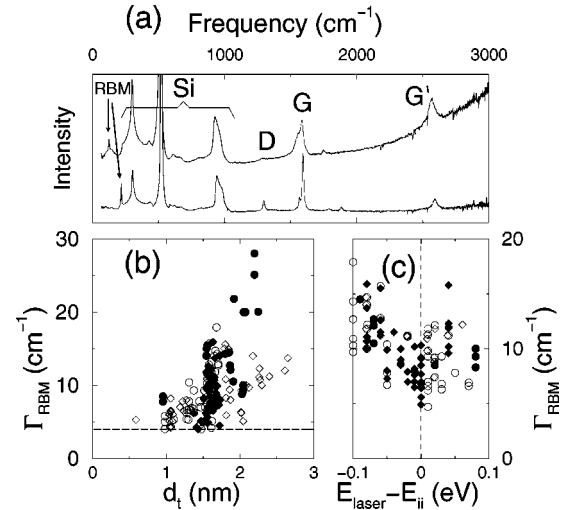
were used in the measurements, one with a high nanotube density (~ 6.0 SWNTs/μm^2) and the other with a low density (~ 0.4 SWNTs/μm^2). Use of the low-density sample essentially guarantees that the resonant Raman signal observed in one light spot (~ 1 μm^2) comes from only one resonant SWNT. Resonance Raman spectra from 170 SWNTs (89 semiconducting and 81 metallic) were acquired. From these data, 73 spectra come from the low-density sample, including 21 from metallic and 52 from semiconducting isolated SWNTs resonant with the incident photons. In this case, all the Raman features are expected to appear in the resonant Raman spectra, and we can then carry out a diameter dependence study of the linewidth for each Raman feature, utilizing the RBM spectra ($\omega_{RBM} = 248/d_t$) for characterizing the structure of the SWNT.[8] We used three laser lines [$E_{laser} = 1.58$ eV (785 nm) from a Ti:sapphire laser and 2.41 eV (514 nm) and 2.54 eV (488 nm) from an Ar ion laser] to observe the Raman spectra for metallic and semiconducting SWNTs resonant with these laser lines over the entire range of tube diameters d_t present in the sample ($\sim 0.9 < d_t < 3.0$ nm). Most of the spectra from isolated SWNTs were acquired using a Renishaw (1000B) micro-Raman spectrometer, although some spectra were acquired using a Kayser (Hololab 5000R). Temperature-dependent Raman measurements on SWNT bundles were performed using a Dilor XY micro-Raman spectrometer. A backscattering configuration was used for all the Raman measurements.

All the experimentally determined linewidth [full width at half maximum (FWHM)] values, which are denoted by Γ,
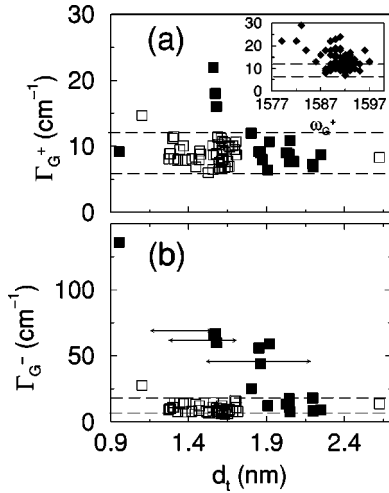
FIG. 3. (a) Γ_{G^+} and (b) Γ_{G^-} for metallic (solid squares) and semiconducting (open squares) SWNTs obtained with the low-density sample. The horizontal arrow lines show results for SWNT bundles, from Ref. 22. The dashed lines indicate the lower and upper values $\Gamma_{G^+} = 6$ cm^{-1} and $\Gamma_{G^+} = 12$ cm^{-1} in (a) and $\Gamma_{G^-} = 6$ cm^{-1} and $\Gamma_{G^-} = 18$ cm^{-1} in (b). The inset plots Γ_{G^+} as a function of the peak frequency ω_{G^+} for SWNTs for the high-density sample and $E_{laser} = 1.58$ eV.

are obtained through a Lorentzian fit of the spectra, with the exception of the Breit-Wigner-Fano (BWF) G-band feature that is observed for the lower-frequency (ω_{BWF}^-) mode for metallic SWNTs. Though it is known that the D and G' bands appear in the Raman spectra of graphitelike materials through a double-resonance process,[9,10] where inhomogeneous broadening occurs, we use the Lorentzian fit as an approximation to estimate their linewidth values (see discussion in Sec. IV C). The instrument function is limited by the grating/CCD, and each CCD pixel represents about 2 cm^{-1} for the 1800 grove/mm grating. Although the large ensemble of Raman spectra was obtained using different Raman spectrometers, different slits and optical alignments, generally speaking, when cutting the slits down to 10 or 5 μm, the triangular shape (3 pixels, $\sim$3.5 cm^{-1} FWHM) stays constant. For slits of 20–50 μm the instrument function shape broadens by up to 5.2 cm^{-1}. We normally use a 20-μm slit, which represents a small increase in the instrument function of about 0.3 cm^{-1}. The linewidth results presented in Figs. 1–4 are the observed values without correcting for the in-
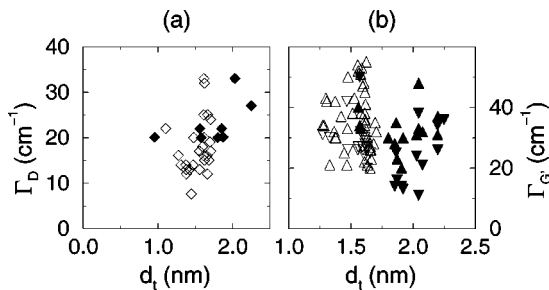

FIG. 4. (a) FWHM linewidth Γ_D and (b) $\Gamma_{G'}$ vs d_t for metallic (solid symbols) and semiconducting (open symbols) SWNTs.

strumental broadening. The small correction due to the instrument function is not important for most of the qualitative analysis discussed in this paper. However, deconvolution of the observed signals with the instrumental function does give us an instrumental linewidth broadening between 1 and 2 cm^{-1} depending on experimental conditions, and this instrumental linewidth broadening is taken into account in this work in cases where it is necessary.

Most of the results discussed here were obtained at room temperature, with samples exposed to air, but Raman measurements were also performed at high and low temperatures on SWNT bundles ("bucky paper" obtained from CarboLex) and on seven isolated SWNTs. Raman spectra from SWNT bundles, for temperatures from 110 K up to 610 K, were performed using a Fluid Inc. cryostat that uses a liquid nitrogen coolant. The laser power impinging on the sample was kept constant (1 mW focused with a 50× objective). Raman spectra from seven isolated SWNTs at $T = 85$ K were obtained using a liquid-nitrogen-cooled cold finger cryostat and a constant incident laser power of 10 mW focused with a 50× objective.

III. TEMPERATURE-DEPENDENT MEASUREMENTS

Resonance Raman spectra between 110 K and 610 K were obtained from SWNT bundles. Figure 1 shows the Raman spectra for SWNT bundles at low and high temperatures for (a) the RBM, (c) the G band, and (e) the G' band. The spectra were obtained with $E_{laser} = 2.41$ eV, where predominantly semiconducting SWNTs are resonant for our SWNT samples. The frequencies increase with decreasing temperature, as expected, primarily due to the softening of the force constants with increasing temperature.[11] The relative intensity of the RBM lines is observed to change with temperature [see Fig. 1(a)], reflecting a possible dependence of E_{ii} on temperature, where E_{ii} denotes the energy of a van Hove singularity in the joint density of electronic states of a nanotube.[1] The measured FWHM linewidths Γ for the several bands are temperature dependent, with Γ increasing by increasing the temperature. The right side of Fig. 1 [plots (b), (d), and (f)] shows the temperature-dependent behavior of the linewidths, corresponding to the spectra in (a), (c), and (e), respectively. For all the Raman features, the decrease in the linewidth with decreasing temperature is faster for $T > 400$ K, and it is very modest for lower temperatures, $T < 400$ K. Small changes of the Γ_{RBM} in SWNT bundles are observed for the entire temperature range. The interpretation is that Γ_{RBM} for the sharpest RBM features in SWNT bundles is determined primarily by the presence of many peaks, each coming from different (n,m) SWNTs with nearly the same diameters, as discussed by Iliev *et al.*[5]

We also performed low-temperature measurements ($T = 85$ K) on seven isolated SWNTs. No significant linewidth changes were observed for these isolated SWNTs comparing the Γ values at $T = 290$ K with the Γ values at $T = 85$ K, consistent with the small change in linewidth for $T < 400$ K observed in SWNT bundles, as shown in Figs. 1(b), 1(d), and 1(f). We conclude that there is little evidence for a T-dependent effect on the linewidth of the various Ra-

man features in isolated SWNTs below room temperature, consistent with the very high in-plane Debye temperature for graphitic materials (2480 K).[12]

IV. ROOM-TEMPERATURE MEASUREMENTS

The results from Sec. III suggest that at room temperature, anharmonic effects and other strongly temperature-dependent scattering mechanisms [processes (i)] are not important mechanisms for the broadening of the Raman features of SWNTs. Therefore, the linewidths of the Raman bands at room temperature reflect the natural linewidths in the absence of other broadening mechanisms, such as from fast resonance Raman processes,[13] and from temperature-independent linewidth broadening effects [processes (ii)]. Therefore, we focus the remaining discussion on processes (ii) which can be studied at room temperature for each Raman feature by examining spectra from many individual isolated SWNTs and their dependence on nanotube structure. We discuss each Raman feature separately, since each feature is affected by different broadening mechanisms. The RBM (Sec. IV A) exhibits a strong linewidth dependence on diameter and resonance condition. The G-band linewidth broadening (Sec. IV B) is mainly related to curvature and Breit-Wigner-Fano interaction effects. The Raman scatterings of both the RBM and G-band are single-resonance scattering mechanisms. Section IV C discusses briefly the D and G' bands that appear in the Raman spectra of SWNTs through a double-resonance Raman scattering mechanism, exhibiting very different linewidth behaviors when compared to the RBM and G-band modes. We use the notation Γ to denote the experimentally fitted value for the half width at half maximum (HWHM) linewidths and γ to denote the smallest observed linewidths for each feature, and we identify γ with the natural linewidth for that feature (after correcting for the instrumental broadening).

A. Radial breathing mode

The radial breathing mode feature [see peaks in Fig. 2(a) below 250 cm^{-1}] is a fully symmetric Raman-allowed mode characteristic of SWNTs, which is, however, not present in graphite. Figure 2(b) shows the dependence of the RBM linewidth (Γ_{RBM}) on diameter d_t for 81 metallic and 89 semiconducting SWNTs. It is noteworthy that Γ_{RBM} values down to 4 cm^{-1} are observed (close to the instrumental function FWHM). This is a small linewidth value when compared to Raman spectra from other graphitelike materials[14,15] and is characteristic of the 1D nature of SWNTs.

By deconvolving the instrument function with the measured profile for the smallest Γ_{RBM} value we obtain an estimate for the natural linewidth ($\gamma_{RBM} \simeq 3$ cm^{-1}) for the resonance Raman scattering by the RBM in SWNTs, in agreement with the value of 3 cm^{-1} reported by Iliev *et al.* based on SWNT bundles.[5] A similar $\gamma_{RBM} = 4$ cm^{-1} value was independently used by Milnera *et al.*[16] to theoretically analyze their experimental results from SWNT bundles. The larger Γ_{RBM} values observed for other SWNTs are related to linewidth broadening effects primarily due to temperature-

independent effects [processes (ii)], as discussed below. For most of these data, the measured linewidths are large enough that the instrument function correction is not important within the accuracy of the reported linewidths.

From the 170 data points in Fig. 2(b), we clearly observe an increase in the average Γ_{RBM} value with increasing d_t, i.e., with increasing number of atoms along the circumference of the SWNTs. This result can be explained by the larger number of phonon and electronic states, i.e., a smaller amount of quantum confinement for phonons and electrons as the diameter increases. For larger diameter tubes, the energy difference between the van Hove singularities decreases, the amplitudes of the singularities decrease, and their widths increase [processes (iib)]. The Γ_{RBM} diameter-dependent broadening must also be related to the disappearance of the RBM feature as d_t increases, explaining why low-frequency RBMs are not usually observed.[3] In the Raman spectra for isolated SWNTs, we rarely observe RBM features below 100 cm^{-1}, although SWNTs with $d_t > 248/100 = 2.48$ nm are not rare in our samples.

Another important factor determining the linewidths is the resonance condition [processes (iic)]. Regarding the temporal behavior of the broadening process for excitation frequencies exactly in resonance with an electronic transition, the scattering time is expected to be much slower than off resonance, reflecting the lifetime of the intermediate state involved. For intermediate-state frequency shifts away from resonance (preresonance condition), the behavior is much more complex, reflecting fundamental uncertainty principle limitations and leading to faster relaxation processes.[17] For SWNTs with a similar d_t, the electronic transition energies E_{ii} are different for different chiral angles θ, due to the trigonal warping effect.[18] Departures from satisfying the resonance condition perfectly contribute to the linewidth, as discussed below.

To study the processes (iic), we plot Γ_{RBM} vs ($E_{laser} - E_{ii}$) in Fig. 2(c) for both semiconducting and metallic SWNTs in the diameter range $1.4 < d_t < 1.8$ nm (we use an overlap energy value $\gamma_0 = 2.89$ eV in calculating E_{ii}). As can be seen in Fig. 2(b), our samples contain many resonant SWNTs in the small diameter region $1.4 < d_t < 1.8$ nm.[8] By using $E_{laser} = 1.58$ eV, *metallic* SWNTs in the d_t range $1.4 < d_t < 1.8$ nm are in a good resonance condition ($E_{laser} \sim E_{ii}$), while *semiconducting* SWNTs in this diameter range are in a good resonance condition when using $E_{laser} = 2.41$ eV. The linewidths for both metallic and semiconducting SWNTs range from $4 < \Gamma_{RBM} < 18$ cm^{-1} for $1.4 < d_t < 1.8$ nm. The smallest Γ_{RBM} values (which lead to our estimate for the natural linewidth γ_{RBM}) occur under the strongest resonance conditions where ($E_{laser} - E_{ii}$) ≈ 0, and the average Γ_{RBM} value in Fig. 2(c) increases as $|E_{laser} - E_{ii}|$ increases. These results show that Γ_{RBM} is smallest under strong resonance conditions and that Γ_{RBM} is broader when a weaker preresonance condition is satisfied for states where E_{ii} deviates from E_{laser}. A stronger contribution to the Raman intensity occurs from the very high density of electronic states closest in energy to the van Hove singularities, E_{ii}. It is also significant that Γ_{RBM} increases more rapidly

for $E_{\text{laser}} < E_{ii}$ than for $E_{\text{laser}} > E_{ii}$, thus reflecting the asymmetry in the van Hove singularity lineshape with respect to E_{ii}.[1,19]

In Fig. 2(c) we see that, for SWNTs with similar diameter and with similar $(E_{\text{laser}} - E_{ii})$ values and even for SWNTs assigned with the same (n,m) indices, there is a spread in the Γ_{RBM} values up to 8 cm^{-1} from the lowest (natural) linewidth value. Since these observed linewidth broadening effects are not related to any SWNT property or to the resonance condition, we conclude that they are associated with extrinsic SWNT broadening processes (iia). We therefore attribute this spread of up to 8 cm^{-1} to broadening processes connected with point defects, finite-size effects, tube deformations, tube-substrate interactions, or roughness in the substrate surface and similar effects. Therefore, although linewidth measurements at the single nanotube level are delicate, measurement of a large number of samples makes it possible to separate the intrinsic from the extrinsic SWNT properties that cause line broadening.

B. Tangential modes: *G* band

1. Isolated SWNTs

To study the diameter dependence of Γ_G for the graphite-like symmetry-allowed G-band modes (and of the other features, as well), we consider the Raman spectra obtained from the low-density sample, in resonance with the incident light (total of 73 spectra), so that we also obtain the corresponding RBM feature for each tube, and therefore an (n,m) assignment can be made for each nanotube.[8] Figure 3 shows the diameter dependence of the linewidths $\Gamma_{\omega_{G^+}}$ and $\Gamma_{\omega_{G^-}}$ for isolated semiconducting (open squares) and metallic (solid squares) SWNTs. Here Γ_{G^+} denotes the linewidth for G^+ that is usually the most intense G-band spectral feature and has a diameter-independent frequency, appearing at $\omega_{G^+} \sim 1591$ cm^{-1},[20] while Γ_{G^-} denotes the linewidth for G^- that is usually the second most intense G-band spectral feature.[20]

The Γ_G values observed for 1D isolated individual SWNTs are generally lower than the corresponding observed values for 3D highly oriented pyrolytic graphite (HOPG) ($\Gamma_{\text{HOPG}} \sim 13$ cm^{-1}). The lowest value observed for both Γ_{G^+} and Γ_{G^-} is 6 cm^{-1}, which we identify with the natural linewidth $\gamma_{G^+} \simeq \gamma_{G^-} \simeq 5$ cm^{-1} (taking instrumental broadening into account). The value $\gamma_G \simeq 5$ cm^{-1} is small, even when compared with $\gamma_{\text{RBM}} \simeq 3$ cm^{-1} (5 cm^{-1} is 0.3% of ω_G, while 3 cm^{-1} is about 2% of ω_{RBM}).

Γ_{G^+} is mostly observed from 6 cm^{-1} up to 12 cm^{-1} [see Fig. 3(a)] without any measurable dependence on diameter or $(E_{\text{laser}} - E_{ii})$, in contrast to the Γ_{RBM} behavior. This result indicates that the diameter-dependent linewidth spread of the first-order Raman modes is strongly related to the radial motion. The observed G-band linewidth deviation from the lowest 6 cm^{-1} value is, then, related to extrinsic SWNT properties (iia processes). Therefore, the smallest observed Γ_{G^+} value (leading to γ_{G^+}) is close to γ_{RBM}, and the maximum linewidth is close to the linewidth for the 1582 cm^{-1} peak in HOPG (~ 13 cm^{-1}) for Γ_{G^+}.

Larger Γ_{G^+} values (up to 30 cm^{-1}) were observed in the high-density sample obtained with $E_{\text{laser}} = 1.58$ eV. The inset to Fig. 3(a) shows Γ_{G^+} data for 89 SWNTs in the high-density sample, so that for these SWNTs the diameter cannot be assigned by the RBM. In the inset we plot Γ_{G^+} as a function of the peak frequency ω_{G^+}. There are two explanations for the observation of the higher Γ_{G^+} values in this inset: first, in a high-density sample, nanotubes close to each other by less than the laser wavelength can interact, causing line broadening (see Ref. 21). Second, most of the results obtained with the high-density sample and $E_{\text{laser}} = 1.58$ eV (shown in the inset) are from metallic SWNTs with diameters in the range $1.44 < d_t < 1.74$ nm. Therefore, although $\gamma_{G^+} \simeq 5$ cm^{-1} for both semiconducting and metallic SWNTs, we conclude that metallic tubes show a larger spread in Γ_{G^+} than semiconducting SWNTs, which seems also to be the case for the Γ_{RBM} data at higher d_t values [see Fig. 2(b)]. Furthermore, a low-density sample must be used to avoid tube-tube interactions.

However Γ_{G^-} for the circumferential-tangential G^- mode gets broader in comparison to Γ_{G^+} for the axial mode. For semiconducting SWNTs, Γ_{G^-} values up to 18 cm^{-1} are observed [see Fig. 3(b)]. The differences can be understood considering the axial (G^+) vs circumferential (G^-) directions of the atomic motions of these tangential modes, indicating that some broadening mechanism is induced in Γ_{G^-} by the presence of curvature (even when there are no conduction electrons), since curvature admixes some out-of-plane graphene modes. In the case of metallic SWNTs, the difference between G^+ and G^- is much stronger due to the coupling between plasmons and the G^- vibrational mode in metallic SWNTs. Figure 3(b) shows that $\Gamma_{G^-_{\text{BWF}}}$ for metallic SWNTs (solid squares) increases with decreasing d_t. This result is known from resonance Raman studies on SWNT bundles,[22] and it is attributed to an increase of the BWF coupling between phonons and plasmons, which occurs with increasing nanotube curvature and decreasing diameter.[22] More discussion about the BWF feature is presented in the next section, in connection with SWNT bundle results for $\Gamma_{G^-_{\text{BWF}}}$.

2. SWNT bundles

To analyze the Raman linewidths in SWNT bundles we need to consider that we are measuring a convolution of peaks from several different metallic and semiconducting SWNTs.[5] In the case of the G band, the picture is still less clear, since we often cannot separate the contributions from the modes with different symmetries.[3,23]

The minimum Γ_{G^+} value of ~ 15 cm^{-1} observed for SWNT bundles[3] is consistent with contributions from the smallest Γ_{G^+} linewidth value of 6 cm^{-1} plus contributions from the diameter-independent frequencies ω_{G^+} of different isolated SWNTs that appear always inside an 8 cm^{-1} frequency range ($\omega_{G^+} = 1591 \pm 4$ cm^{-1}) for both semiconducting and metallic SWNTs.[20] One mechanism that could account for the additional linewidth usually observed in Γ_{G^+} for most SWNT bundles[3] might be due to tube-tube interac-

tion, as indicated by polarization measurements on isolated SWNTs with a close-lying neighboring SWNT.[21]

For Γ_{G^-} in SWNT bundles, the strong diameter dependence (Ref. 20) and the presence of a nonresolved E_2 mode are the main mechanisms responsible for the inhomogeneous broadening of this feature, which shows up as a convolution of different ω_{G^-} frequencies related to the SWNT diameter distribution in the sample. This broadening gets even larger because of the presence of some resonant *metallic* SWNTs (with larger BWF linewidths) in a bundle that is generally in resonance with semiconducting tubes using $E_{laser} = 2.41$ eV.

The horizontal arrow lines in Fig. 3(b) show $\Gamma_{G_{BWF}^-}$ for metallic SWNTs obtained from three SWNT bundles with different diameter distributions, taken from Ref. 22. Good agreement in $\Gamma_{G_{BWF}^-}$ is observed between isolated SWNTs and SWNT bundles within the same diameter range ($\sim 1.35 \leqslant d_t \leqslant \sim 1.85$ nm). However, the apparently linear dependence of $\Gamma_{G_{BWF}^-}$ vs d_t shown in Ref. 22 seems not to be valid over a wide range of d_t, showing serious deviation for lower ($d_t < 1$ nm) and higher ($d_t > 2$ nm) tube diameters. For $d_t > 2$ nm, $\Gamma_{G_{BWF}^-}$ is observed to be below 18 cm^{-1} [which is the usual maximum Γ_{G^-} value for isolated semiconducting SWNTs; see Fig. 3(b)], indicating that the BWF coupling is not effective for such large diameter tubes. This result is consistent with the G^- Lorentzian-like line shape observed for these features for SWNTs with large ($d_t > 2$ nm) tube diameters.[20,22] Therefore, for SWNTs with larger d_t values, phonons and plasmons coexist with little interaction, as is the case for graphite. For SWNTs with diameters near the boundary where 1D plasmons are stable, a strong interaction between phonons and plasmons occurs, and rapid changes in line shape with d_t can take place. Finally, SWNTs with d_t below 1 nm represent an overdamped case where the phonon gets heavily broadened and downshifted.[24] Furthermore, tube-tube interactions might be responsible for some of the differences observed between the $\Gamma_{G_{BWF}^-}$ results for isolated SWNTs compared to SWNT bundles.[25,26] The Breit-Wigner-Fano effect in SWNT bundles is stronger than in isolated SWNTs, as can be concluded from the larger intensity of the BWF G-band component observed in SWNT bundles.[20,24] Further experimental and theoretical studies are necessary to clarify the importance of tube-tube interaction in the Breit-Wigner-Fano coupling.

C. Disorder-induced D band and its G'-band overtone

Figure 4 shows the diameter dependence for Γ_D and $\Gamma_{G'}$, the D- and G'-band linewidths, respectively [see also Fig. 2(a)]. The D band is a disorder-induced band and it is observed in about half of the spectra from isolated SWNTs. The G' band does not require the presence of defects and is also observed in highly crystalline HOPG, since the G'-band mechanism is a second-order process involving two D-band phonons, with $+q$ and $-q$ momenta, thus satisfying momentum conservation. The G' band is observed for all the SWNTs (including semiconducting, metal-1 and metal-2 tubes[1]), different from the prediction that only metal-2 SWNTs exhibit D bands[27] and therefore also G' bands. De-

pending on the resonance process, one peak (up triangles) or two peaks (up and down triangles) are observed in the G' band,[28,29] and when the two peaks are unresolved, this process can be a source of line broadening. The trigonal warping effect, when unresolved is another broadening mechanism for metallic SWNTs.[29]

Due to the disorder-induced origin of the D band, Γ_D changes dramatically from sample to sample in sp^2 carbons, and Γ_D can be larger than 100 cm^{-1} in highly disordered sp^2 carbons.[12,30] Some bulk sp^2 graphitic materials, such as P1 pyrocarbon, with a strong 2D character, exhibit a relatively low Γ_D for an sp^2 carbon of $\Gamma_D \sim 30$ cm^{-1}.[31] In this context, the small linewidth Γ_D observed for the D band in some isolated SWNTs, going down to 7 cm^{-1}, is especially noteworthy, and this smallest D-band linewidth (implying $\gamma_D \simeq 6$ cm^{-1} after accounting for instrumental broadening) is identified with the natural D-band linewidths. The smallest $\Gamma_{G'}$ observed for SWNTs is 11 cm^{-1}, leading to our estimate of $\gamma_{G'} \simeq 10$ cm^{-1}. In comparison, the G' band is observed in 2D P1 pyrocarbon with linewidths $\Gamma_{G'} = 42$ cm^{-1},[31] while in HOPG, two G' peaks are observed due to the interlayer interaction, and these peaks exhibit linewidths $\Gamma_{G'} = 42$ cm^{-1} and 34 cm^{-1}.[31] For highly defective sp^2 carbon materials, $\Gamma_{G'}$ exhibits much higher values, going up to ~ 150 cm^{-1}.[31]

By comparing Fig. 4 with Figs. 2 and 3, it can be clearly seen that there is a qualitatively different mechanism for the Raman scattering processes involving the RBM and G band (regular resonance Raman scattering) compared to processes involving the D and G' bands (double-resonance Raman scattering[9,10]). A broad distribution of linewidths up to 56 cm^{-1} and down to 11 cm^{-1} was observed for $\Gamma_{G'}$ in isolated SWNTs, compared to a relatively small spread for the RBM and G-band linewidths. No evident dependence of $\Gamma_{G'}$ on diameter or chirality was observed.

The crystalline disorder is an important factor responsible for the Γ_D and $\Gamma_{G'}$ linewidths. But for SWNTs with low defect densities (such as SWNTs with very low D-band intensity or unobservable D bands), the linewidths are expected to depend on the physical origin of these scattering processes. The D-band and G'-band linewidths in sp^2 carbon materials are naturally broader when compared to the first-order Raman G-band mode in graphite or in SWNTs and to the RBM in SWNTs, due to the double-resonance nature of the scattering processes for the D and G' bands. In the double-resonance Raman process, a range of phonons with different wave vectors q is involved, giving rise to Raman scattering at different frequencies. This process causes an inhomogeneous line broadening and the Raman features do not actually have perfect Lorentzian line shapes. In the case of SWNTs, the van Hove singularities limit the wave vectors that strongly contribute to the D-band and G'-band spectral features, thereby giving rise to small natural linewidths, as low as $\gamma_D \simeq 6$ cm^{-1} and $\gamma_{G'} \simeq 10$ cm^{-1}, and a large spread in Γ_D and $\Gamma_{G'}$ values, as observed in Fig. 4. For a quantitative analysis of Γ_D and $\Gamma_{G'}$, more experimental and theoretical work is necessary.

V. SUMMARY

We analyzed the room-temperature linewidths Γ for the RBM, G-band, D-band, and G'-band Raman features observed for 170 isolated SWNTs. Low-temperature (<290 K) Raman measurements show no significant temperature-dependent change in the linewidths near room temperature, indicating that phonon-phonon–phonon-electron scattering events are not so important in the determination of the linewidths at room temperature. Although linewidth measurements on a single-nanotube level are delicate, the measurement of a large number of samples allows us to separate intrinsic and extrinsic SWNT properties (e.g., substrate roughness) contributing to the Raman linewidths.

All the Raman features exhibit very small *natural* linewidths for this 1D material when compared to 2D and 3D graphitic materials. The RBM shows a significant broadening that increases with increasing diameter, explaining why low-frequency RBM modes (below 100 cm^{-1}) in SWNTs and MWNTs (multiwall nanotubes) are usually not observed. The RBM shows also a clear dependence on how well the resonance condition of E_{laser} with the 1D van Hove singularities is obeyed.

The deviations from the natural linewidth for SWNTs with similar diameters and chiralities reflect line broadening effects due to extrinsic SWNT properties. These line broadening effects are shown to be different for the G^+ and G^- peaks in the G band, reflecting a broadening effect due to nanotube curvature for the G^- feature. In the case of metallic SWNTs, the coupling of the G^- phonon with plasmons strongly increases the linewidth of the lower-frequency feature G_{BWF}^-. The phonon-plasmon coupling depends on the curvature, and the experimental $\Gamma_{G_{\text{BWF}}^-}$ data show different regimes for the plasmon-phonon coupling.

The D and G' bands exhibit very different linewidth results when compared to the RBM and G-band modes, in agreement with the double-resonance nature of these features. The presence of very small Γ_D and $\Gamma_{G'}$ values provides strong evidence for a sharp selectivity of q vectors due to the confinement of electrons and phonons in 1D SWNTs. Theoretical study of the linewidths of the D band and the G' band are likely to be very informative about the details of the double-resonance process in SWNTs and how it differs from that in 2D graphite. In general, theoretical models are necessary for a more quantitative analysis of the linewidths of all four features in the SWNT Raman spectra discussed in this paper.

[1] R. Saito, G. Dresselhaus, and M.S. Dresselhaus, *Physical Properties of Carbon Nanotubes* (Imperial College Press, London, 1998).

[2] M.S. Dresselhaus, G. Dresselhaus, and Ph. Avouris, *Carbon Nanotubes: Synthesis, Structure, Properties and Applications*, Vol. 80 of Springer Series in Topics in Applied Physics (Springer-Verlag, Berlin, 2001).

[3] M.S. Dresselhaus and P.C. Eklund, Adv. Phys. **49**, 705 (2000).

[4] M.S. Dresselhaus, G. Dresselhaus, A. Jorio, A.G. Souza Filho, and R. Saito, Carbon (to be published).

[5] M.N. Iliev, A.P. Litvinchuk, S. Arepalli, P. Nikolaev, and C.D. Scott, Chem. Phys. Lett. **316**, 217 (2000).

[6] We include both the contributions labeled γ (2 cm^{-1}) and Γ_0 (1 cm^{-1} for $T=0$) to obtain an estimate for the natural linewidth in Ref. 5.

[7] J.H. Hafner, C.L. Cheung, T.H. Oosterkamp, and C.M. Lieber, J. Phys. Chem. B **105**, 743 (2001).

[8] A. Jorio, R. Saito, J.H. Hafner, C.M. Lieber, M. Hunter, T. McClure, G. Dresselhaus, and M.S. Dresselhaus, Phys. Rev. Lett. **86**, 1118 (2001).

[9] C. Thomsen and S. Reich, Phys. Rev. Lett. **85**, 5214 (2000).

[10] R. Saito, A. Jorio, A.G. Souza Filho, G. Dresselhaus, M.S. Dresselhaus, and M.A. Pimenta, Phys. Rev. Lett. **88**, 027401 (2002).

[11] H.D. Li, K.T. Yue, Z.L. Lian, Y. Zhan, L.X. Zhou, S.L. Zhang, Z.J. Shi, Z.N. Gu, B.B. Liu, R.S. Yang, H.B. Yang, G.T. Zou, Y. Zhang, and S. Iijima, Appl. Phys. Lett. **76**, 2053 (2000).

[12] M.S. Dresselhaus, G. Dresselhaus, K. Sugihara, I.L. Spain, and H.A. Goldberg, *Graphite Fibers and Filaments*, Vol. 5 of Springer Series in Materials Science (Springer-Verlag, Berlin, 1988).

[13] A. Weber, *Raman Spectroscopy in Gases and Liquids*, Topics in Current Physics Vol. 11 (Springer-Verlag, Heidelberg, 1979).

[14] A.C. Ferrari and J. Robertson, Phys. Rev. B **61**, 14 095 (2000).

[15] M.S. Dresselhaus and R. Kalish, *Ion Implantation in Diamond, Graphite and Related Materials*, Springer Series in Materials Science (Springer-Verlag, Berlin, 1992), Vol. 22.

[16] M. Milnera, J. Kürti, M. Hulman, and H. Kuzmany, Phys. Rev. Lett. **84**, 1324 (2000).

[17] D.L. Rousseau, J.M. Friedman, and P.F. Williams, *Raman Spectroscopy of Gases and Liquids*, edited by A. Weber (Springer-Verlag, Berlin, 1979), Vol. 11, pp. 1–20.

[18] R. Saito, G. Dresselhaus, and M.S. Dresselhaus, Phys. Rev. B **61**, 2981 (2000).

[19] A. Jorio, A.G. Souza Filho, G. Dresselhaus, M.S. Dresselhaus, R. Saito, J.H. Hafner, C.M. Lieber, F.M. Matinaga, M.S.S. Dantas, and M.A. Pimenta, Phys. Rev. B **63**, 245416 (2001).

[20] A. Jorio, A.G. Souza Filho, G. Dresselhaus, M.S. Dresselhaus, A.K. Swan, B. Goldberg, M.S. Ünlü, M.A. Pimenta, J.H. Hafner, C.M. Lieber, and R. Saito, Phys. Rev. B **65**, 155412 (2002).

[21] A. Jorio, A.G. Souza Filho, V.W. Brar, A.K. Swan, M.S. Ünlü, B.B. Goldberg, A. Righi, J.H. Hafner, C.M. Lieber, R. Saito, G. Dresselhaus, and M.S. Dresselhaus, Phys. Rev. B **65**, 121402 (2002).

[22] S.D.M. Brown, A. Jorio, P. Corio, M.S. Dresselhaus, G. Dresselhaus, R. Saito, and K. Kneipp, Phys. Rev. B **63**, 155414 (2001).

[23] A. Jorio, G. Dresselhaus, M.S. Dresselhaus, M. Souza, M.S.S. Dantas, M.A. Pimenta, A.M. Rao, R. Saito, C. Liu, and H.M. Cheng, Phys. Rev. Lett. **85**, 2617 (2000).

[24] Gerald D. Mahan, *Many-Particle Physics (Physics of Solids and Liquids)*, 3rd. ed. (Kluwer Academic, New York, 2000).

[25] H. Kataura, Y. Kumazawa, N. Kojima, Y. Maniwa, I. Umezu, S. Masubuchi, S. Kazama, Y. Ohtsuka, S. Suzuki, and Y. Achiba, J. Mol. Liq. Cryst. **340**, 757 (2000).

[26] C. Jiang, K. Kempa, J. Zhao, U. Schlecht, U. Kolb, T. Basché, M. Burghard, and A. Mews, Phys. Rev. Lett. (unpublished).

[27] J. Maultzsch, S. Reich, and C. Thomsen, Phys. Rev. B **64**, 121407 (2001).

[28] A.G. Souza Filho, A. Jorio, Anna K. Swan, M.S. Ünlü, B.B. Goldberg, R. Saito, J.H. Hafner, C.M. Lieber, M.A. Pimenta, G. Dresselhaus, and M.S. Dresselhaus, Phys. Rev. B **65**, 085417 (2002).

[29] A.G. Souza Filho, A. Jorio, Ge.G. Samsonidze, G. Dresselhaus, M.S. Dresselhaus, A.K. Swan, B.B. Goldberg, M.S. Ünlü, R. Saito, J.H. Hafner, C.M. Lieber, and M.A. Pimenta, Chem. Phys. Lett. **354**, 62 (2002).

[30] A.C. Ferrari and J. Robertson, Phys. Rev. B **64**, 075414 (2001).

[31] H. Wilhelm, M. Lelaurian, E. McRae, and B. Humbert, J. Appl. Phys. **84**, 6552 (1998).